THE JOURNAL OF PHYSICAL CHEMISTRY B

Article

pubs.acs.org/JPCB

Structure and Conductivity of Semiconducting Polymer Hydrogels

Rachel C. Huber,[†] Amy S. Ferreira,[†] Jordan C. Aguirre,[†] Daniel Kilbride,[†] Daniel B. Toso,[‡] Kenny Mayoral,[†] Z. Hong Zhou,[‡,§] Nikos Kopidakis,[∥] Yves Rubin,[†] Benjamin J. Schwartz,[†,§] Thomas G. Mason,[†] and Sarah H. Tolbert*[,†,§]

[†]Department of Chemistry and Biochemistry, UCLA, Los Angeles, California 90095-1569, United States

[‡]Department of Microbiology, Immunology & Molecular Genetics, and Biomedical Engineering Program, UCLA, 609 Charles E. Young Drive South, Los Angeles, California 90095, United States

[§]California NanoSystems Institute, UCLA, 570 Westwood Plaza, Los Angeles, California 90095, United States

[∥]Chemical and Nanoscience Center, National Renewable Energy Laboratory, 15013 Denver West Parkway, Golden, Colorado 80401, United States

[#]Department of Materials Science and Engineering, UCLA, Los Angeles, California 90095, United States

Supporting Information

ABSTRACT: Poly(fluorene-*alt*-thiophene) (PFT) is a conjugated polyelectrolyte that self-assembles into rod-like micelles in water, with the conjugated polymer backbone running along the length of the micelle. At modest concentrations (~10 mg/mL in aqueous solutions), PFT forms hydrogels, and this work focuses on understanding the structure and intermolecular interactions in those gel networks. The network structure can be directly visualized using cryo electron microscopy. Oscillatory rheology studies further tell us about connectivity within the gel network, and the data are consistent with a picture where polymer chains bridge between micelles to hold the network together. Addition of tetrahydrofuran (THF) to the gels breaks those connections, but once the THF is removed, the gel becomes stronger than it was before, presumably due to the creation of a more interconnected nanoscale architecture. Small polymer oligomers can also passivate the bridging polymer chains, breaking connections between micelles and dramatically weakening the hydrogel network. Fits to solution-phase small-angle X-ray scattering data using a Dammin bead model support the hypothesis of a bridging connection between PFT micelles, even in dilute aqueous solutions. Finally, time-resolved microwave conductivity measurements on dried samples show an increase in carrier mobility after THF annealing of the PFT gel, likely due to increased connectivity within the polymer network.

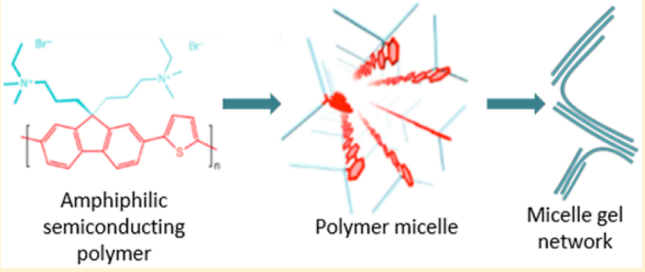

1. INTRODUCTION

Conjugated polyelectrolytes (CPEs) are a class of polymers that consist of a π-conjugated backbone with ionic pendant groups.[1−4] Due to their charged side chains, CPEs can self-assemble into various motifs, including nanoparticles[5−7] and rods.[4,8,9] This assembly is driven by the kinetics of polymer aggregation in various solvents and can result in changes of the polymer's physical and electronic properties, including the polymer's absorption[10,11] and conductivity.[8] Because assembly offers control over such a range of properties, these materials have been integrated into OPVs,[12−14] sensors,[15,16] and biomedical imaging.[17−19] We have also used the rod-like CPE that is the focus of this work to create assemblies with water soluble fullerenes that upon photoexcitation lead to extremely long-lived separated charges (polarons) that do not recombine for days to weeks.[20]

CPEs also have the ability to form hydrogels if the building blocks self-assemble into extended structures, in much the same way that molecules like cetyltrimethylammonium bromide (CTAB) can be induced to form long worm-like micelles that result in gel formation.[21] Polymer hydrogels consist of a three-dimensional (3-D) network held together by either chemical or physical means. A chemical hydrogel requires cross-linkers to create an interconnected network,[22−24] whereas a physical hydrogel network is held together by electrostatic interactions, van der Waals forces, hydrogen bonds, and so forth.[25,26] In this work, we specifically examine a novel type of hydrogel network where polymer micelles are connect by bridging polymer chains that coassemble with multiple micelles, resulting in a robust gel network.

The sub-10 nm structure of most gel networks is challenging to characterize through standard methods such as transmission electron microscopy (TEM) because these disordered networks

Special Issue: William M. Gelbart Festschrift

Received: March 2, 2016
Revised: April 12, 2016
Published: April 14, 2016

DOI: 10.1021/acs.jpcb.6b02202
J. Phys. Chem. B 2016, 120, 6215−6224

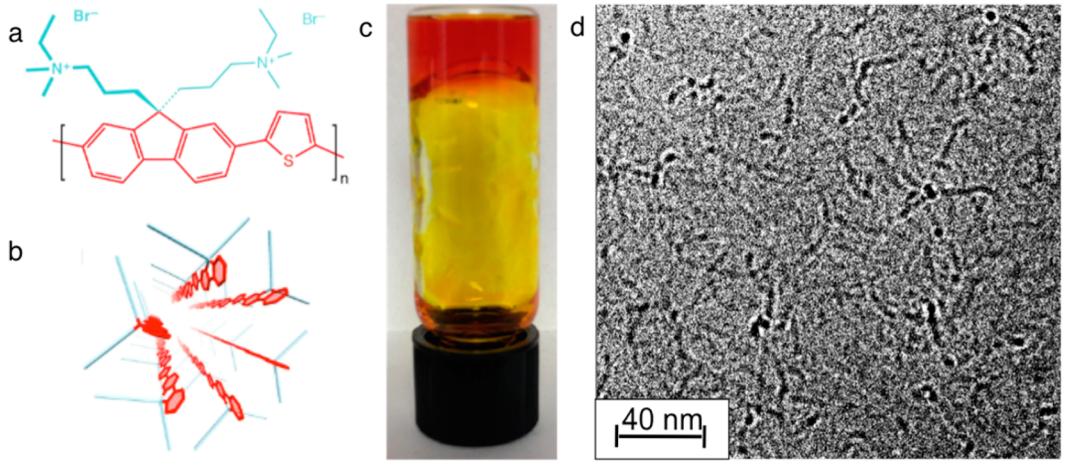

Figure 1. Properties of PFT. (a) Chemical structure of the PFT monomer. (b) Cartoon of an assembled PFT micelle based on SAXS and cryoEM data. (c) Photograph of an upside-down vial of a PFT hydrogel, demonstrating the solid nature of the gel. (d) cryoEM image of PFT micelles showing the connected nature of the micelles even at dilute concentrations (1 mg/mL).

lack both periodicity and electron density contrast, as they consist mainly of carbon, and the structure can change upon drying. To address this problem, in this work, we use cryo electron microscopy (cryoEM) to observe the existence of an interconnected network of rod-like micelles for a CPE. This is then complemented by solution-phase small-angle X-ray scattering (SAXS), Dammin bead modeling, and rheology measurements, all of which are indirect methods used to test hypothetical real-space models of the hydrogel's structure.

The gel structure of CPEs is essential to their implementation in electronic devices. For example, in organic photovoltaics (OPVs), a continuous nanostructured polymer network is required for extraction of charges out of the devices.[27] If discontinuous networks form due to polymer aggregation kinetics or phase separation from a second OPV component, then photogenerated current is lost. Thus, the advantage of forming fully interconnected polymer networks from self-assembling CPEs is that this provides a route to create thermodynamically stable films with a beneficial function for optoelectronic devices.

In this study we show that the CPE, poly(fluorene-*alt*-thiophene) (PFT; see Figure 1 for the chemical structure) self-assembles into a network of cylindrical micelles in solution. CryoEM provides a visualization of the polymer micelles that form in dilute solutions. Using solution SAXS in combination with Dammin bead modeling, we are able to determine the average size and shape of the micelles as well as the branching structure. Oscillatory mechanical rheometry is then used to measure the viscoelastic moduli and yielding behavior of the polymer network, and from this measured strength, we are able to postulate the types of connections that promote PFT gel network formation. We next show that the gels become stronger upon annealing with tetrahydrofuran (THF) and use Dammin bead modeling to visualize the annealing process. Finally, time-resolved microwave conductivity (TRMC) is used to show how THF annealing increases charge carrier mobility through the gel network.

2. EXPERIMENTAL SECTION

Polymer synthesis was performed as previously reported.[8] To further purify the PFT into high- and low-molecular-weight (MW) fractions, 250 mg of PFT was dissolved in 5 mL of DMSO. Once dissolved, ethyl acetate was added to the PFT/DMSO solution until the polymer began to precipitate out of solution. Centrifugation was then used to pull the precipitated PFT out of the suspended solution. After pouring off the solution and drying the PFT, the solid that remained had a fairly high MW, and for the rest of this paper, we refer to this fraction as high-MW PFT. More ethyl acetate was then added to the remaining solution, and the rest of the polymer precipitated out of solution, producing the fraction that we refer to as low-MW PFT. All structural and rheological studies were then performed on samples made by dissolving this size-separated PFT in water at various concentrations.

THF annealing of aqueous PFT solutions was performed by adding 0.05 mL of THF to 0.5 mL of H_2O containing various amounts of PFT. PFT gels became liquid upon addition of THF. The THF was then removed by heating and stirring the sample at 80 °C for 4 h. Any water evaporated in this process was added back to the solution to keep the total polymer concentration constant before and after THF annealing.

CryoEM imaging grids for TEM were prepared by placing a small drop (~4 μL) of sample solution onto a glow-discharged holey-carbon mesh (Quantifoil 200 mesh grids) with 3.5 μm holes spaced 1 μm apart. The grids were then blotted and plunged immediately into liquid-nitrogen-cooled liquid ethane to rapidly freeze the samples into vitrified ice. The cryoEM grids were visualized with an FEI Tecnai F20 transmission electron microscope with an accelerating voltage of 200 kV. Images were collected at ~50 000× magnification with a underfocus of approximately 3 μm.

SAXS experiments were conducted at the Stanford Synchrotron Radiation Lightsource (SSRL) on Beamline 4-2. Using a syringe, 100 μL of each sample was loaded into a quartz capillary and held at 25 °C. Scattered X-rays (at 12 keV) were collected with a Rayonix MX225-HE detector (sample to detector distance = 1.7 m). The 2-D data were radially averaged to obtain 1-D scattering curves.

Raw solution SAXS data were fit and smoothed using Gnom, and bead modeling was performed on the smoothed data using Dammin, a Monte Carlo type modeling software that uses beads and solvent to create shapes that could have generated the experimental curves. The expert setting was used, and the bead size was set to have a radius of 5 Å, corresponding to the width of a single polymer chain. The diameter of the sphere was

DOI: 10.1021/acs.jpcb.6b02202
J. Phys. Chem. B 2016, 120, 6215−6224

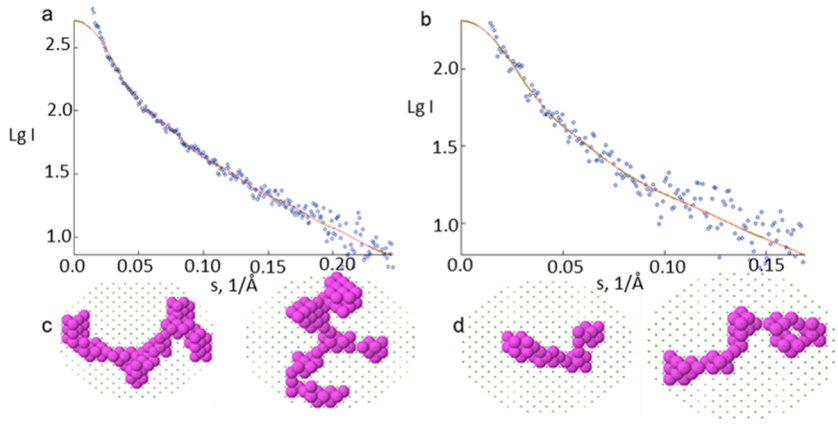

Figure 2. Fits of raw SAXS data to Dammin bead models for (a) 1 mg/mL high-MW PFT samples and (b) 1 mg/mL low-MW PFT samples. The corresponding bead models show a more bridged network in (c) the high-MW PFT sample, whereas the low-MW PFT sample (d) shows what appears to be single micelles that are not branched. Additional bead models are available in the SI.

set to be 140 Å. Each data set was run at least five times to ensure that trends were reproducible. Only a subset of the overall data is shown in the figures.

Rheological properties were measured on a Rheometrics RFS2 strain-controlled rheometer. The geometry used was the cone-and-plate for both strain-sweep and frequency-sweep experiments. Strain-sweep measurements were performed at a frequency of ω = 1 rad/s, and the frequency-sweep measurements were performed at a shear strain of γ = 5%, corresponding to the linear response regime.

Flash photolysis TRMC was used to measure photoconductivity via methods that have been previously reported.[28−31] Briefly, samples for microwave conductivity measurements were deposited onto 10 × 24 mm quartz substrates that were cleaned by subsequent ultrasonic baths in detergent, deionized water, acetone, and isopropanol for 10 min each. Samples were placed into an X-band microwave cavity terminated with a grating that is transparent to optical excitations but reflective to microwaves. The samples were excited through the quartz substrates by a 5 ns, 500 nm laser pulse produced from an optical parametric oscillator (Continuum Panther) pumped by the 355 nm harmonic of a Q-switched Nd:YAG laser (Continuum Powerlite) with a typical fluence of 0.56 mJ/cm^2. The intensity of the excitation was controlled by switchable neutral density filters. The photoinduced carries absorbed the incident microwaves, and the change in microwave power was measured and related to the conductance, ΔG, of the sample.[32] From ΔG, the product of the yield of the free charge carriers generated per photon absorbed, φ, with the sum of the mobilities of these carriers, $\sum\mu$, can be calculated as $\varphi\sum\mu = \Delta G/(\beta q_e I_0 F_A)$,[32] where I_0 is the photon flux of the excitation beam incident on the sample, F_A is the fraction of absorbed photons at the excitation wavelength, β = 2.2 is a geometric factor, and q_e is the elementary charge.

3. RESULTS AND DISCUSSION

The chemical structure of PFT is shown in Figure 1a. This CPE can form micelles in water because of its amphiphilic character and because each monomer unit has an overall wedge shape with a large hydrophilic volume and a small hydrophobic volume; the hydrophilic volume stems from the tetrahedral carbon on the fluorene unit where the charged side chains attach.[8,33] These factors, combined with the fairly linear nature of the PFT backbone, allow PFT to assemble into rod-like micelles where the backbone of PFT runs along the long axis of the micelle, as shown by the cartoon illustration in Figure 1b. The assembly of these charged PFT polymer chains into micelles keeps the hydrophobic polymer backbone away from the aqueous solvent without forcing the polymer to coil into enthalpically unfavorable conformation that breaks the π-bonding in the polymer backbone. Despite the loss of conformational entropy in the polymer micelle, assembly is entropically favorable because when hydrophobic groups come into contact with water, they generally cause ordering of the water in order to preserve the aqueous hydrogen bond network and thus decrease the entropy of water. The PFT structure was characterized in detail for low-MW material in our previous work.[8]

For higher MW samples, at concentrations as low as 10 mg/mL, PFT forms a hydrogel, as seen in the photograph of the inverted vial shown in Figure 1c. The MW of the PFT is critical to the formation of the gel network; thus, size-selective precipitation was used to obtain both high- and low-MW fractions of the synthesized material, as described above. While the high-MW polymer readily gels, the low-MW polymer does not form a gel network, indicating that the interactions between polymer micelles in the gel network depend on the polymer chain length. Unless explicitly stated otherwise, all of the experiments described below use only the high-MW polymer fraction.

3.A. Direct Structural Characterization of PFT Gels Using CryoEM and SAXS. Using cryoEM on dilute aqueous PFT solutions (Figure 1d), we can observe both the micellar nature of the PFT assemblies and interconnections between those micelles, which should lead to hydrogel formation at higher concentrations. The cryoEM samples were prepared by flash-freezing a droplet of PFT solution, as described above. The images produced show both micelles that are in the plane of the image, which appear as rods, and micelles standing on end, which appear as darker spots. From this data, we can measure the diameter of the micelles to be about 4 nm, a size that correlates well with solution SAXS data published previously.[8] The cryoEM data provides clear evidence for PFT micelle formation and for the formation of interconnections between micelles, but because of the limited region that can be imaged at one time, it does not provide good statistical data on the average structure of the sample as a whole.

DOI: 10.1021/acs.jpcb.6b02202
J. Phys. Chem. B 2016, 120, 6215−6224

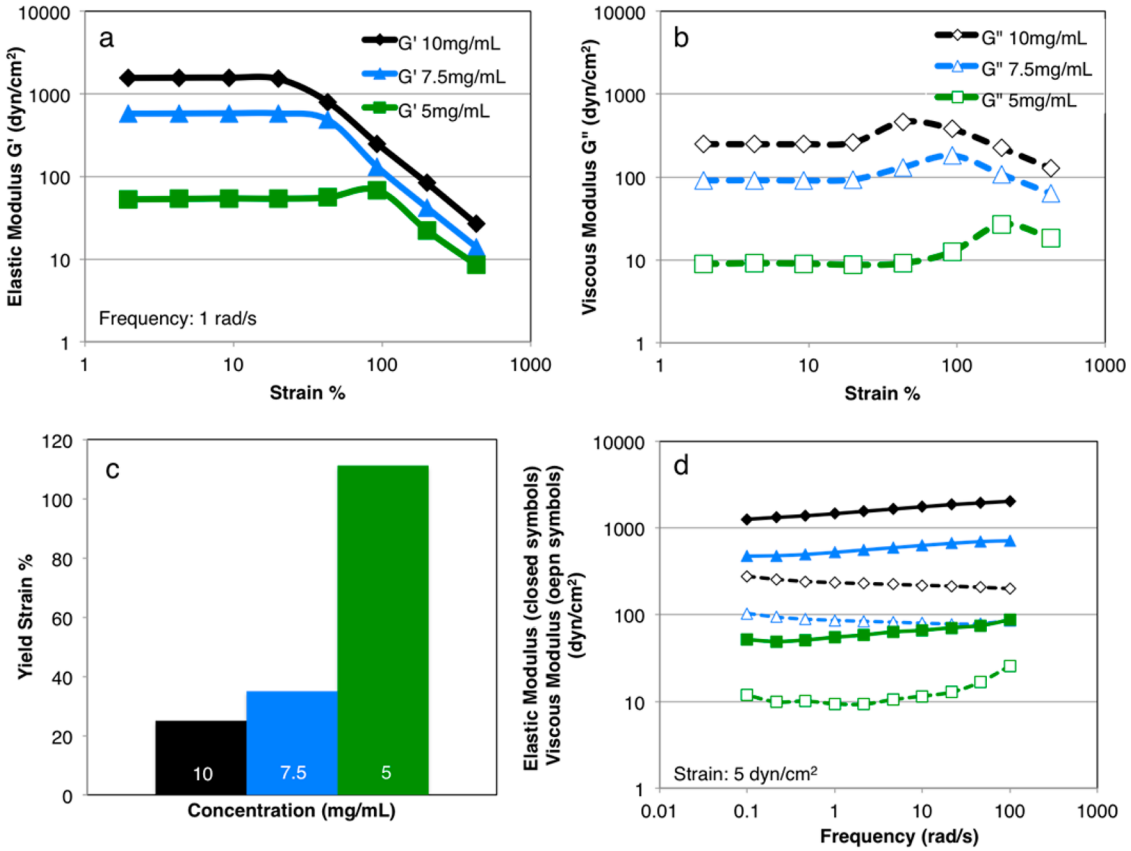

Figure 3. Mechanical shear rheometry measurements of gels with concentrations of 10, 7.5, and 5 mg/mL. (a) The strain-dependent elastic modulus and (b) the strain-dependent viscous modulus show that the most concentrated samples result in the strongest gel networks. (c) The yield strain (the point where enough strain has been applied to the system that it flows and is no long by definition a solid) is shown as a function of gel concentration. Softer gels yield at higher strains. (d) The frequency-dependent elastic and viscous moduli, showing the characteristics of hydrogels with robust networks.

To further study the structure of the PFT micelle system, we thus turned to solution SAXS. Solution SAXS has been used extensively to examine the nanometer-scale structure of assemblies in solution.[34−36] By fitting the scattered intensity to a power law, $I = q^{-\alpha}$, we can relate the exponential slope, α, to the structure of the polymer in solution. Figure 2a shows that the scattering from high-MW PFT fits to two distinct slopes: α = 1.5 at low q and α = 3.7 at high q. The low-q slope of 1.5 is indicative of a rod-like shape at large distances, concomitant with the length of a rod; the high-q slope of 3.7 is indicative of a sphere-like shape, concomitant with the radius of the rod. This SAXS-determined rod-like shape correlates well with the micelle shapes observed by cryoEM. Similar power law behavior can also be seen for low-MW PFT (Figure 2b).

Along with the power law analysis, the data can also be fit with a bead model to learn more about the detailed network structure. To do this, the raw data can be fit using the software Gnom to enable smoothing of the data before bead model analysis. The Dammin bead model fits this smoothed data and outputs a structure that is in statistical agreement with the scattering data.[37] Comparing bead model fits for aqueous solutions of high- and low-MW PFT (Figure 2c and d, respectively, with more bead model fits shown in Figure S1 of the SI) indicates that the network formed by the high-MW PFT has a more branched structure than that formed by low-MW PFT. As stated above, the low-MW polymer does not form a gel, while the high-MW PFT does. From this data, we thus postulate that the low-MW polymer is present mostly in the form of discrete polymer micelles, while the high-MW PFT forms a branched network that leads to gel formation. The base unit of this polymer hydrogel, as indicated by cryoEM, SAXS, and these Dammin bead model fits, is a rod-shaped polymer micelle.

3.B. Understanding Connections in the Gel Network via Rheology. With the basic structural element in hand, we now turn to rheology measurements to help determine how that polymer network is held together. Rheology is the study of the deformation or flow of matter and is one of the most useful techniques for studying the physics of a gel network.[38] The two components of the linear complex viscoelastic modulus, G^*, are the elastic storage modulus (G', the in-phase or real part) and the viscous loss modulus (G'', the 90° out-of-phase part). The storage modulus reflects the material's capacity to elastically store energy resulting from shear excitations, and the loss modulus reflects its capacity to dissipate energy.[39] Strictly speaking, G' and G'' are well-defined only at very small strains (γ) in the linear response regime, but it is customary to measure these properties for very large strains beyond the yield point and still refer to them as G' and G'', even in the nonlinear regime. Solids typically have $G' > G''$ over a large frequency (ω) range, extending to low frequencies. At fixed ω, constant behavior of $G'(\gamma)$ and $G''(\gamma)$ in the limit of small γ indicates linear behavior; at larger γ beyond the linear regime, a drop-off in $G'(\gamma)$ and a peak in $G''(\gamma)$ signify yielding behavior, beyond which dominantly viscous flow occurs at very high strains. By studying the viscoelastic response of a CPE hydrogel under

DOI: 10.1021/acs.jpcb.6b02202
J. Phys. Chem. B 2016, 120, 6215−6224

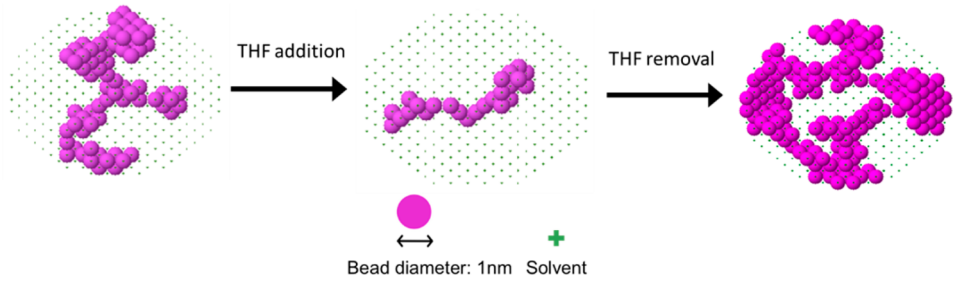

Figure 4. Dammin bead models from SAXS experiments (see the SI) on samples of high-MW PFT before THF annealing, after addition of THF, and after THF removal. Before THF annealing, the high-MW PFT shows a branched morphology. Upon addition of THF, however, the gel structure disassembles to either single PFT micelles or individual polymer chains. When THF is removed, the system shows an even higher polymer density that is representative of a more branched gel network.

various strain and frequency studies, we can infer a great deal about the structure of the gel network.

We begin our rheology experiments with a gedanken model for the structure of the gel network and then attempt to prove or disprove that model. Given the micellar nature of PFT in solution, the very low concentrations where PFT begins to gel, and the fact that PFT has no significant potential to make either covalent or hydrogen bonds between polymer chains, we hypothesize that it is the micelle formation itself that results in gel formation. For example, single linear polymer chains can be incorporated into two different micelles, linking the micelles together in much the same way that bridging actin fibers connect actin bundles in actin gel networks.[40] We can describe these bridging polymer chains as "sticky ends" because in the absence of a second PFT micelle, a dangling polymer chain end likely to adopt a high-energy, coiled conformation in aqueous solution, which would prefer to associate with another polymer micelle.

We can study the response of these PFT hydrogels under constant strain or constant frequency to help determine the PFT network structure. Figure 3a and b shows the values of $G'(\gamma)$ and $G''(\gamma)$ as a function of strain amplitude at a constant frequency of 1 rad/s for gels with concentrations of 10, 7.5, and 5 mg/mL. As expected, both the $G'(\gamma)$ and $G''(\gamma)$ values of the PFT gel increase as the polymer concentration increases, indicating that more concentrated gels have more interconnections. The elastic storage modulus for PFT shows a linear viscoelastic regime, where the modulus does not change with strain amplitude. The 10 and 7.5 mg/mL samples both show a decrease in $G'(\gamma)$ at large strains, which indicates yielding. As expected, the yield point is higher for the softer 7.5 mg/mL gel. The softest 5 mg/mL hydrogel yields the highest strains and shows a peak in $G'(\gamma)$ before $G'(\gamma)$ decreases and the gel begins to flow; at that point, $G''(\gamma)$ is significantly larger than $G'(\gamma)$. For all samples, $G''(\gamma)$ begins with a linear viscoelastic regime but has an increase or peaks at high strains before decreasing similarly to $G'(\gamma)$.

Structurally, the elastic modulus $(G'(\gamma))$ reflects the number density of junctions in the polymer network, whereas the viscous modulus $(G''(\gamma))$ can reflect relaxation of elastic structures such as entanglements or connections that are being broken and formed dynamically under entropic microscopic excitations. The peak observed in $G''(\gamma)$ for all samples is indicative of the yield point of a dominantly elastic material, where the shear excitations far exceed entropic excitations and elements within the material are excited by the shear strain into shapes that are no longer similar to those at thermal equilibrium. For $G'(\gamma)$, if the polymer chains that bridge between micelles are disrupted, it should create more unbound sticky ends, which should be loosely coiled due to steric constraints.[41] Because the 10 and 7.5 mg/mL samples are too concentrated to allow the polymer chains to reorient, an increase in $G'(\gamma)$ at high γ is not observed before the material yields. This behavior is common in many polymer solutions and hydrogels.[42,43] In contrast, the 5 mg/mL samples show strain hardening in $G'(\gamma)$; this increase in the elastic moduli is expected because lower concentrations mean fewer connections between micelles and thus a weaker PFT network. When a large enough strain is applied to the system, it disrupts both the polymer micelles and the network. The sticky ends can then reorient to bridge with other micelles in a more ideal configuration, resulting in an increase in the number of junctions of this system. The observation of strain hardening in $G'(\gamma)$ as lower concentration is thus constant with the idea that bridging polymer chains are responsible for the formation of the PFT network.

Another important parameter that we can take from this polymer rheology study is the yield strain % of the gel. The yield strain % of the hydrogel, shown in Figure 3c, is the point where the strain amplitude applied to the system is sufficient to cause the network to break so that the entire system begins to flow (the stress/strain curves that were used to determine the yield strain % are available in Figure S2 of the SI).[44] In the case of PFT micelles, the bridging polymer chains would need to detach from one micelle, allowing the samples to become liquid-like. There is only a slight difference between the yield strain percentages for the 10 and 7.5 mg/mL gels. However, the 5 mg/mL gel has a yield strain that is more than twice as high as the 10 and 7.5 mg/mL gels. This increase in yield strain % results from the lower density network that has the ability to dynamically reform junctions as strain is applied. Thus, the conclusions about the network from examining the yield strain % of the gel agree well with the conclusions gleaned above from the elastic and viscous moduli.

Frequency-dependent measurements can be used to gain further insight about the nature of the gel. The frequency study in Figure 3d was performed at a constant strain amplitude of 5%, chosen to be in the plateau region for all gel samples. As in the strain amplitude measurements, we find that $G'(\omega)$ is always higher than $G''(\omega)$, proving that we have a solid-like gel. Also, as higher-frequency oscillations are applied to the PFT gel, the slopes of the curves remain close to zero. This lack of response with increased frequency is also characteristic of physical gels because the network is strong enough to resist changes.[36] This implies that even though these are not exceptionally strong gels, the interactions that hold the gels

DOI: 10.1021/acs.jpcb.6b02202
J. Phys. Chem. B 2016, 120, 6215−6224

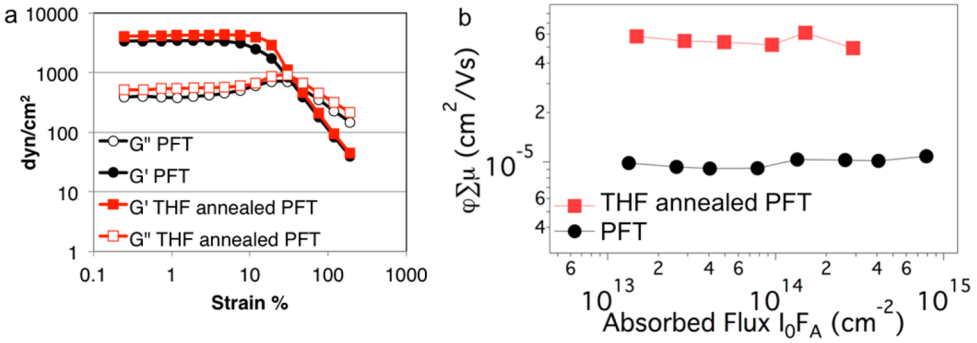

Figure 5. (a) Strain-dependent curves comparing high-MW PFT gels before (black) and after THF annealing (red). An increase is observed in both $G'(\gamma)$ and $G''(\gamma)$, suggesting a more robust network after THF annealing. (b) TRMC photoconductances measured on dried films cast from high-MW PFT solutions; films were cast before (black) and after THF annealing (red). Because the number of carriers created is not expected to change, the data show that THF annealing provides an overall increase in carrier mobility.

together are quite robust. The viscous modulus for the 5 mg/mL sample does vary more with frequency than do those for the 10 and 7.5 mg/mL samples, likely due to the fact that the 5 mg/mL sample contains a much less connected gel, and therefore, it is easier to reorient the micelles in this sample at high frequencies. These frequency measurements thus provide further information about the bridged PFT network.

3.C. THF Annealing of PFT Hydrogels. Studying the chemical factors that destroy these PFT hydrogels also can provide information about what holds them together. For example, the gel network is destroyed when aqueous PFT solutions are exposed to THF.[45] Upon removal of the THF from the polymer system by thermal evaporation, the gel network reforms. We hypothesize that this behavior arises because THF can enthalpically stabilize the coiled sticky ends of polymer chains that used to bridge between micelles, allowing the system to break the connections between micelles.

The THF annealing process for PFT hydrogels can be followed by SAXS and analyzed with Dammin bead modeling as well as rheology. Figure 4 shows representative bead models for PFT samples before THF annealing, with THF present, and after removal of the THF (more bead models are available in Figures S3 and S4 of the SI). The effect of adding THF to the aqueous micelle system is clearly observed by the loss of branching in the micelle network. The width of the structure decreases to approximately the width of a single bead, indicating that THF causes the solution to become either single solvated PFT chains or much smaller micelles. Upon removal of the THF, the PFT network becomes stronger, with the plateau modulus increasing from 3380 to 4080 dyn/cm^2, as seen in Figure 5a. Apparently, the gel network reforms in a more interconnected state than it is able to attain initially, presumably because network formation is kinetically limited when samples are first prepared. In agreement with this idea, Dammin modeling indicates that upon removal of the THF, both the branched structure and the width of the polymer micelles are restored (the raw scattering data with fit is available in the SI, Figure S4). Interestingly, the branching density increases, indicating that the postannealed gel network contains more interconnected polymer micelles, compared to its preannealed counterpart. Thus, both the SAXS and rheological studies support the idea that THF-annealed PFT gels have a more interconnected network.

If THF annealing increases the density of network connections, then it follows that THF annealing should also increase the conductivity of the PFT network. TRMC is a unique tool that allows for measurement of the photoconductivity of solid-state films without a need for electrical contacts.[46,47] In TRMC, photoinduced carriers are created by a laser pulse incident on the sample. These mobile carriers then absorb microwaves as they are induced to move by the microwave electric field, and the change in microwave power is measured. The change in microwave power is proportional to the local nanometer-scale photoconductivity of the sample, which is the product of the mobile carrier yield per photon absorbed, φ, and the sum of the mobilities of the carriers, $\sum\mu$ (the carriers in this case are both electrons and holes, as discussed in the Experimental Section).

Figure 5b shows that films produced from PFT solutions (diluted from gels) that have been THF-annealed have a 6-fold increase in the $\varphi\sum\mu$ product. If we assume that the carrier yield is comparable in all of the PFT gel samples (a reasonable assumption given their identical chemical nature and absorption of the pump laser), then the carrier mobility must be higher in the THF-annealed sample. We attribute this increased mobility in part to the increased number of connections between polymer micelles, as observed in Dammin bead models and discussed above. In addition, it is likely that THF annealing also decreases chain coiling and thus increases the intrinsic polymer mobility. While we do not have any direct structural measure of polymer chain conformation, increased bridging likely means that some chains that were coiled are now bridging between micelles. Moreover, it has been shown that kinks and bends in polymer chains cause trap sites that reduce carrier mobility.[48,49] Extending the conjugation length of the polymer by having longer straight sections has also been shown to increase charge carrier mobility at microwave frequencies.[50] The significant increase in microwave conductivity thus suggests that in addition to making more interconnections between micelles, THF annealing may also increases the polymer ordering within micelles, a fact that is consistent with the observed increase in the plateau modulus.

3.D. Understanding Gel Network Structure via Mixing of Low- and High-MW PFT. Although all of the experiments described above provide information about the nature of these PFT hydrogels, they do not concretely prove that bridging polymer chains act as sticky ends that link micelles together. Thus, to further investigate this idea, we can take advantage of the fact that the polymer synthesis provides us with both high- and low-MW fractions (obtained by size-selective precipitation, as discussed above). To this end, we selectively recombined the high- and low-MW PFT with different ratios but maintained

DOI: 10.1021/acs.jpcb.6b02202
J. Phys. Chem. B 2016, 120, 6215−6224

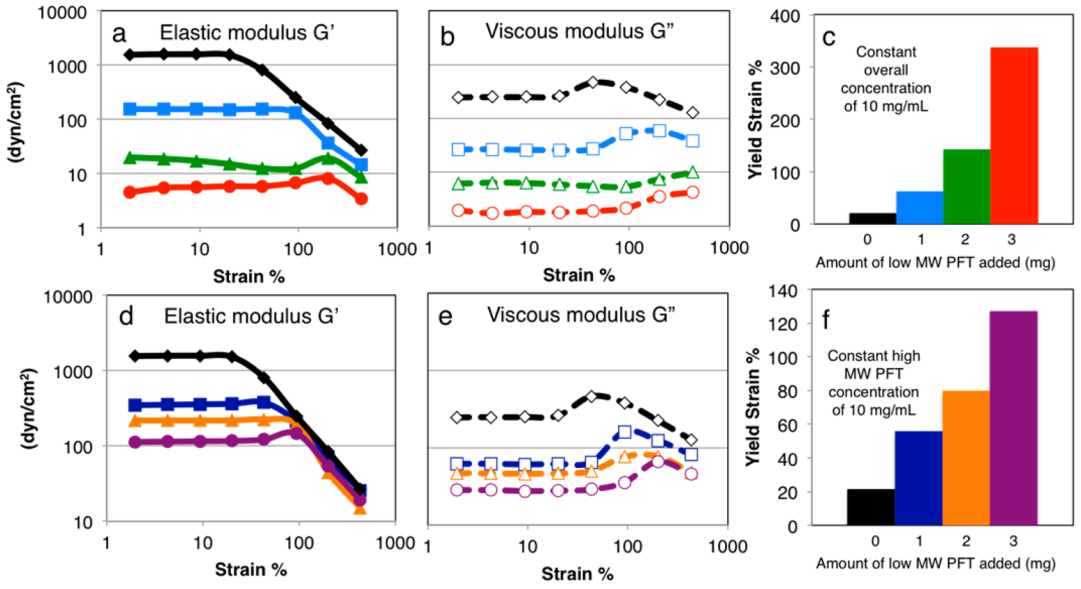

Figure 6. Rheological studies of PFT hydrogels made using various mixtures of low- and high-MW polymer. (a–c) Strain-dependent elastic modulus (a), viscous modulus (b), and yield strain (c) for PFT hydrogel made with a constant total polymer concentration (10 mg/mL) but different ratios of low-MW PFT to high-MW PFT. As more low-MW PFT is added, the hydrogel strength decreases, implying that the low-MW PFT is decreasing the amount of bridging polymer chains in the sample. (d–f) Strain-dependent elastic modulus (d), viscous modulus (e), and yield strain (f) for hydrogel samples made with a fixed concentration (10 mg/mL) of high-MW PFT combined with various amounts of low-MW PFT (1, 2, and 3 mg/mL). As low-MW PFT is added to high-MW PFT, the strength of the hydrogel decreases even though the overall polymer concentration is increasing.

the same overall polymer concentration. In this way, we can test how the low-MW PFT, which does not form a gel, interacts with the gel-forming high-MW PFT.

Figure 6a and b shows $G'(\gamma)$ and $G''(\gamma)$, respectively, for a series of samples that all have a total PFT concentration of 10 mg/mL but are made up of different fractions of low- and high-MW polymer. The samples contain polymer ratios of 9 mg high-MW PFT to 1 mg of low-MW PFT (9:1), 8 mg high-MW PFT to 2 mg of low-MW PFT (8:2), and 7 mg of high-MW PFT to 3 mg of low-MW PFT (7:3). As a control, we also made a pure high-MW 10 mg/mL PFT sample (10) that has no low-MW PFT; this sample forms the strongest gel and thus provides a standard of comparison for the mixed-MW PFT samples. The figure shows clearly that there is an order of magnitude decrease in the plateau modulus between the 10 mg/mL and the 9:1 samples and another order of magnitude decrease between the 9:1 and 8:2 samples. The plateau modulus for the 7:3 sample is yet another four times lower than that for the 8:2 sample.

This dramatic decrease in the strength of the gel is caused not just by the decreasing amount of high-MW polymer but also by the addition of the low-MW PFT. For example, the pure 7.5 mg/mL high-MW sample in Figure 3a has a $G'(\gamma)$ plateau value of 575 dyn/cm^2, where the 7:3 sample, which contains essentially the same amount of high-MW polymer, has a $G'(\gamma)$ plateau value of just 4.5 dyn/cm^2. We postulate that the reason for the decrease in gel strength is that the low-MW polymer is able to cap or passivate the sticky ends of the high-MW PFT, allowing dangling high-MW polymer chains to achieve an enthalpically favorable conformation without the entropic constraints of bridging between micelles.

We can obtain even more information about the mixed-MW samples by again focusing on the strain hardening observed in the elastic storage modulus (Figure 6a and b). The pure 10 mg/mL PFT samples and the 9:1 samples show only yielding behavior, whereas the 8:2 and 7:3 samples show strain hardening at higher strains. This suggests that there are still sufficient interconnections in the 9:1 sample to prevent dynamical network reformation under strain. However, with the 8:2 and 7:3 samples, the potential bridging polymers from some micelles are capped with the low-MW PFT; therefore, when strain is applied, the remaining polymer bridges are flexible enough to transiently disengage and reform in a more optimized configuration. Moreover, the increase in yield strain % seen in Figure 6c (the stress/strain curves are shown in Figure S5 of the SI) is much more dramatic than the increase found in Figure 3c with increasing gel dilution. This again indicates that low-MW PFT actively interacts with the high-MW polymer to break connection between micelles.

Although the data presented above provides strong indication that low-MW PFT disrupts the gel network, the fact that the total amount of high-MW PFT is not constant in these samples complicates the issue. We thus performed a second set of experiments using a fixed concentration of high-MW PFT and a varying total polymer concentration. For this experiment, the concentration of high-MW PFT was kept at 10 mg/mL, and low-MW PFT was added in 1, 2, and 3 mg amounts (10:1, 10:2, 10:3).

As above, Figure 6d and e shows a decrease of $G'(\gamma)$ and $G''(\gamma)$ upon the addition of low-MW PFT, despite the fact that the total polymer concentration increases. The decrease of the elastic modulus after addition of 1 mg of low-MW PFT is roughly an order of magnitude, although it is less than that observed in Figure 6a for the 9:1 sample. Indeed, the plateau moduli monotonically decrease as more low-MW PFT is added to the system. Normal yielding behavior at high strains in $G'(\gamma)$ is observed for the 10:1 and 10:2 samples, but the 10:3 sample again shows slight strain hardening at high strains. It follows that the 10:1 and 10:2 samples still exhibit significant micelle bridging as the ratio of low/high-MW PFT is not high enough to effectively break up the gel network. However, in the 10:3 samples, enough low-MW PFT is present to passivate the sticky

DOI: 10.1021/acs.jpcb.6b02202
J. Phys. Chem. B 2016, 120, 6215–6224

ends of the polymer micelles and disrupt the network. The yield strain % in Figure 6f also steadily increases as low-MW PFT is added, but the increase is not as large as that in Figure 6c (the stress/strain curves are shown in Figure S5 of the SI). This data thus indicates that both the total concentration of high-MW polymer and the low-MW/high-MW ratio interplay to control the density of connections within the network.

The structural effects of adding low-MW PFT to high-MW PFT were further analyzed using solution SAXS and Dammin bead modeling on dilute 1 mg/mL samples. Figure 7a and b shows fits for the 9:1 and 7:3 and for the 10:1 and 10:3 high-MW/low-MW samples, respectively (see Figures S6–S9 in the SI for additional bead models). When comparing the 9:1 and 7:3 samples, we find that although the total polymer concentration is the same, the density of beads in the two models differs, indicating that in the 7:3 sample, a larger fraction of the polymer chains are individually dissolved (or form very small aggregates that are too small to see in the scattering vector range used for this experiment). The 9:1 sample contains a higher density of beads, indicating larger aggregates in solution and higher branching. The 10:1 and 10:3 samples show a similar trend, even though a higher bead density might have been expected for the 10:3 sample due to the higher total polymer concentration. Indeed, even though the 10:1 sample contains less polymer and the same amount of high-MW PFT as the 10:3 sample, a higher overall bead density is observed, again indicting larger aggregates with increased branching in solution for the 10:1 sample. This supports the idea that low-MW PFT caps the sticky ends of bridging high-MW PFT strands, resulting in less aggregate branching and more linear, single rod structures in samples containing larger amounts of low-MW polymer.

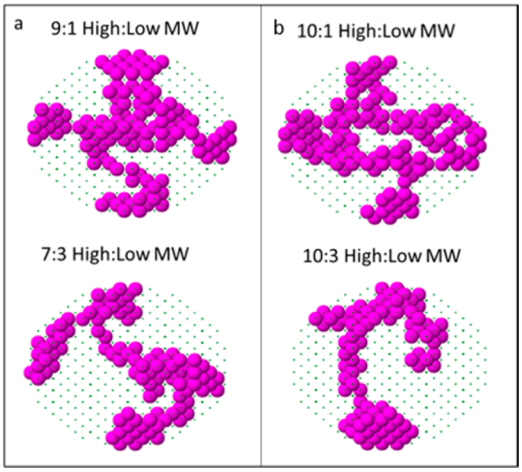

Figure 7. Dammin bead models of SAXS experiments for the same mixed high-MW/low-MW PFT hydrogel samples whose rheology is explored in Figure 6. Samples with a constant overall polymer concentration are shown in (a), and samples with a constant concentration of high-MW PFT are shown in (b). In both (a) and (b), the density of the beads in the fitting box decreases as low-MW PFT is added to the high-MW PFT. This suggests that low-MW PFT caps the sticky ends of the high-MW PFT micelles, creating smaller aggregates that are hard to see in the SAXS experiment. For example, the total polymer concentration of the 10:3 sample is quite a bit higher than that of the 10:1 sample, but the bead density is higher in the less concentrated 10:1 sample because it contains less low-MW polymer and thus larger aggregates.

4. CONCLUSIONS

In this study, we examined the network structure of semiconducting polymer PFT hydrogels. TEM and SAXS were employed to examine the micellar building blocks of the hydrogel, and Dammin models were used to analyze the solution SAXS data to visualize the network structure. All of these data support the hypothesis of a hydrogel network built from rod-like micelle primary units. Rheology was used to examine interconnections within the gel network, and a combination of TRMC and rheology indicated that a more interconnected and potentially more locally ordered network was formed after THF annealing of the gel. Bead models and rheology studies on aqueous solutions of mixed low-MW and high-MW PFT were used to further our understanding of the interactions that hold this semiconducting polymer gel network together. All of the data strongly support a picture where the gel network is held together by polymer chains that bridge neighboring micelles by coassembling with more than one micelle based on amphiphilic interactions. These bridging polymer chains, or sticky ends, can be disrupted by shear force, by the addition of organic solvents such as THF, or by adding low-MW polymers that can coassemble with the sticky ends in a nonbridging fashion.

A key conclusion that comes from this work is the fact that high-MW polymer chains bridge between micelles, offering the potential for facile electrical conductivity within the 3-D gel network. Although direct electrical measurements on the hydrogel network are complicated by the high conductivity of water, our TRMC results on dried networks show great promise for future device applications. The strongly interconnected nature of these conjugated polymer hydrogel networks could be ideal for a variety of polymer-based electronic devices as they rely on good 3-D conductivity in a heterostructured network.

■ ASSOCIATED CONTENT

Supporting Information

The Supporting Information is available free of charge on the ACS Publications website at DOI: 10.1021/acs.jpcb.6b02202.

Additional Dammin bead models for both high- and low-molecular-weight (MW) pure PFT as well as for mixtures of high-MW and low-MW polymer in various ratios, raw SAXS data with Dammin fits for high-MW PFT with and without THF, stress/strain curves used to determine yield strains for pure gels of 5, 7.5, and 10 mg/mL as well as for the full range of mixtures of high/low-MW PFT present in the paper, and data on crossover strain for both pure high-MW PFT at various concentrations and for the full range of mixtures of high- and low-MW PFT (PDF)

■ AUTHOR INFORMATION

Corresponding Author

*E-mail: tolbert@chem.ucla.edu. Tel.: (310)206-4767.

Author Contributions

The first two authors contributed equally.

Notes

The authors declare no competing financial interest.

DOI: 10.1021/acs.jpcb.6b02202
J. Phys. Chem. B 2016, 120, 6215–6224

■ ACKNOWLEDGMENTS

This work was supported by the National Science Foundation under Grant Number CHE-1112569 (synthesis, rheology, TEM, and SAXS Monte Carlo fitting) and by the Center for Molecularly Engineered Energy Materials (MEEM), an Energy Frontier Research Center funded by the U.S. Department of Energy, Office of Science, Basic Energy Sciences under Award Number DE-SC0001342 (TRMC, SAXS data collection). J.C.A. acknowledges the NSF IGERT: Materials Creation Training Program (MCTP), Grant Number DGE-0654431, and the California NanoSystems Institute. This manuscript contains data collected at the Stanford Synchrotron Radiation Lightsource (SSRL). SSRL and the SLAC National Accelerator Laboratory are supported by the U.S. Department of Energy, Office of Science, Office of Basic Energy Sciences under Contract No. DE-AC02-76SF00515. The SSRL Structural Molecular Biology Program is supported by the DOE Office of Biological and Environmental Research and by the National Institutes of Health, National Institute of General Medical Sciences (including P41GM103393). The contents of this publication are solely the responsibility of the authors and do not necessarily represent the official views of NIGMS or NIH. The authors acknowledge the use of instruments at the Electron Imaging Center for NanoMachines supported by NIH (1S10RR23057 to ZHZ) and CNSI at UCLA.

■ REFERENCES

(1) Chi, C.; Mikhailovsky, A.; Bazan, G. C. Design of Cationic Conjugated Polyelectrolytes for DNA Concentration Determination. *J. Am. Chem. Soc.* **2007**, *129*, 11134−11145.

(2) Jiang, H.; Zhao, X.; Schanze, K. S. Effects of Polymer Aggregation and Quencher Size on Amplified Fluorescence Quenching of Conjugated Polyelectrolytes. *Langmuir* **2007**, *23*, 9481−9486.

(3) Jiang, H.; Taranekar, P.; Reynolds, J. R.; Schanze, K. S. Conjugated Polyelectrolytes: Synthesis, Photophysics, and Applications. *Angew. Chem., Int. Ed.* **2009**, *48*, 4300−4316.

(4) Thomas, A.; Houston, J. E.; Van den Brande, N.; De Winter, J.; Chevrier, M.; Heenan, R. K.; Terry, A. E.; Richeter, S.; Mehdi, A.; Van Mele, B.; et al. All-Conjugated Cationic Copolythiophene "rod−rod" Block Copolyelectrolytes: Synthesis, Optical Properties and Solvent-Dependent Assembly. *Polym. Chem.* **2014**, *5*, 3352.

(5) Wu, C.; Bull, B.; Szymanski, C.; Christensen, K.; McNeill, J. Multicolor Conjugated Polymer Dots for Biological Fluorescence Imaging. *ACS Nano* **2008**, *2*, 2415−2423.

(6) Tuncel, D.; Demir, H. V. Conjugated Polymer Nanoparticles. *Nanoscale* **2010**, *2*, 484−494.

(7) Stevens, A. L.; Kaeser, A.; Schenning, A. P. H. J.; Herz, L. M. Morphology-Dependent Energy Transfer Dynamics in Fluorene-Based Amphiphile Nanoparticles. *ACS Nano* **2012**, *6*, 4777−4787.

(8) Clark, A. P.-Z.; Shi, C.; Ng, B. C.; Wilking, J. N.; Ayzner, A. L.; Stieg, A. Z.; Schwartz, B. J.; Mason, T. G.; Rubin, Y.; Tolbert, S. H. Self-Assembling Semiconducting Polymers-Rods and Gels from Electronic Materials. *ACS Nano* **2013**, *7*, 962−977.

(9) Zaroslov, Y. D.; Gordeliy, V. I.; Kuklin, a. I.; Islamov, a. H.; Philippova, O. E.; Khokhlov, a. R.; Wegner, G. Self-Assembly of Polyelectrolyte Rods in Polymer Gel and in Solution: Small-Angle Neutron Scattering Study. *Macromolecules* **2002**, *35*, 4466−4471.

(10) Nguyen, T.; Martini, I.; Liu, J.; Schwartz, B. Controlling Interchain Interactions in Conjugated Polymers: The Effects of Chain Morphology on Exciton-Exciton Annihilation and Aggregation in MEH-PPV Films. *J. Phys. Chem. B* **2000**, *104*, 237−255.

(11) Martini, I. B.; Smith, A. D.; Schwartz, B. J. Exciton-Exciton Annihilation and the Production of Interchain Species in Conjugated Polymer Films: Comparing the Ultrafast Stimulated Emission and Photoluminescence Dynamics of MEH-PPV. *Phys. Rev. B: Condens. Matter Mater. Phys.* **2004**, *69*, 1−12.

(12) Seo, J.; Gutacker, A.; Sun, Y.; et al. Improved High-Efficiency Organic Solar Cells via Incorporation of a Conjugated Polyelectrolyte Interlayer. *J. Am. Chem. Soc.* **2011**, *133*, 8416−8419.

(13) Costa, T.; Marques, A. T.; Seixas de Melo, J.; Thomas, A. W.; Garner, L. E.; Scherf, U.; Bazan, G. C.; Burrows, H. D. Self-Assembly of Poly{1,4-Phenylene-[9,9-bis(4-Phenoxy- Butylsulfonate)]fluorene-2,7-Diyl} with Oppositely Charged Phenylenevinylene Oligoelectrolytes. *J. Phys. Chem. B* **2014**, *118*, 613−623.

(14) He, Z.; Zhong, C.; Su, S.; Xu, M.; Wu, H.; Cao, Y. Enhanced Power-Conversion Efficiency in Polymer Solar Cells Using an Inverted Device Structure. *Nat. Photonics* **2012**, *6*, 593−597.

(15) Lutkenhaus, J. L.; Hammond, P. T. Electrochemically Enabled Polyelectrolyte Multilayer Devices: From Fuel Cells to Sensors. *Soft Matter* **2007**, *3*, 804.

(16) Wang, D.; Gong, X.; Heeger, P. S.; Rininsland, F.; Bazan, G. C.; Heeger, A. J. Biosensors from Conjugated Polyelectrolyte Complexes. *Proc. Natl. Acad. Sci. U. S. A.* **2002**, *99*, 49−53.

(17) Shu, S.; Zhang, X.; Wu, Z.; Wang, Z.; Li, C. Gradient Cross-Linked Biodegradable Polyelectrolyte Nanocapsules for Intracellular Protein Drug Delivery. *Biomaterials* **2010**, *31*, 6039−6049.

(18) O'Connell, M. J.; Chan, C. K.; Li, W.; Hicks, R. K.; Doorn, S. K.; Wang, H.-L. Polyelectrolyte Platform for Sensitive Detection of Biological Analytes via Reversible Fluorescence Quenching. *Polymer* **2007**, *48*, 7582−7589.

(19) Tai, B. C. U.; Wan, A. C. a; Ying, J. Y. Modified Polyelectrolyte Complex Fibrous Scaffold as a Matrix for 3D Cell Culture. *Biomaterials* **2010**, *31*, 5927−5935.

(20) Huber, R. C.; Ferreira, A. S.; Thompson, R.; Kilbride, D.; Knutson, N. S.; Devi, L. S.; Toso, D. B.; Challa, J. R.; Zhou, Z. H.; Rubin, Y.; Schwartz, B. J.; Tolbert, S. H. Long-Lived Photoinduced Polaron Formation in Conjugated Polyelectrolyte/Fullerene Assemblies. *Science* **2015**, *348*, 1340−1343.

(21) Chakraborty, T.; Ghosh, S.; Moulik, S. P. Micellization and Related Behavior of Binary and Ternary Surfactant Mixtures in Aqueous Medium: Cetyl Pyridinium Chloride (CPC), Cetyl Trimethyl Ammonium Bromide (CTAB), and Polyoxyethylene (10) Cetyl Ether (Brij-56) Derived System. *J. Phys. Chem. B* **2005**, *109*, 14813−14823.

(22) Hennink, W. E.; van Nostrum, C. F. Novel Crosslinking Methods to Design Hydrogels. *Adv. Drug Delivery Rev.* **2002**, *54*, 13−36.

(23) Luo, Y.; Kirker, K. R.; Prestwich, G. D. Cross-Linked Hyaluronic Acid Hydrogel Films: New Biomaterials for Drug Delivery. *J. Controlled Release* **2000**, *69*, 169−184.

(24) Peppas, N. a.; Hilt, J. Z.; Khademhosseini, a.; Langer, R. Hydrogels in Biology and Medicine: From Molecular Principles to Bionanotechnology. *Adv. Mater.* **2006**, *18*, 1345−1360.

(25) Campoccia, D.; Doherty, P.; Radice, M.; Brun, P.; Abatangelo, G.; Williams, D. F. Semisynthetic Resorbable Materials from Hyaluronan Esterification. *Biomaterials* **1998**, *19*, 2101−2127.

(26) Prestwich, G. D.; Marecak, D. M.; Marecek, J. F.; Vercruysse, K. P.; Ziebell, M. R. Controlled Chemical Modification of Hyaluronic Acid: Synthesis, Applications, and Biodegradation of Hydrazide Derivatives. *J. Controlled Release* **1998**, *53*, 93−103.

(27) Shaw, P. E.; Ruseckas, A.; Samuel, I. D. W. Exciton Diffusion Measurements in Poly(3-Hexylthiophene). *Adv. Mater.* **2008**, *20*, 3516−3520.

(28) Kroeze, J. E.; Savenije, T. J.; Vermeulen, M. J. W.; Warman, J. M. Contactless Determination of the Photoconductivity Action Spectrum, Exciton Diffusion Length, and Charge Separation Efficiency in Polythiophene-Sensitized TiO 2 Bilayers. *J. Phys. Chem. B* **2003**, *107*, 7696−7705.

(29) Dicker, G.; de Haas, M. P.; Siebbeles, L. D. A.; Warman, J. M. Electrodeless Time-Resolved Microwave Conductivity Study of Charge-Carrier Photogeneration in Regioregular poly(3-Hexylthiophene) Thin Films. *Phys. Rev. B: Condens. Matter Mater. Phys.* **2004**, *70*, 45203.

(30) Piris, J.; Kopidakis, N.; Olson, D. C.; Shaheen, S. E.; Ginley, D. S.; Rumbles, G. The Locus of Free Charge-Carrier Generation in

DOI: 10.1021/acs.jpcb.6b02202
J. Phys. Chem. B 2016, 120, 6215−6224

Solution-Cast Zn1−xMgxO/Poly(3-Hexylthiophene) Bilayers for Photovoltaic Applications. *Adv. Funct. Mater.* **2007**, *17*, 3849−3857.
(31) Ferguson, A. J.; Kopidakis, N.; Shaheen, S. E.; Rumbles, G. Quenching of Excitons by Holes in Poly(3-Hexylthiophene) Films. *J. Phys. Chem. C* **2008**, *112*, 9865−9871.
(32) Savenije, T. J.; Ferguson, A. J.; Kopidakis, N.; Rumbles, G. Revealing the Dynamics of Charge Carriers in Polymer:Fullerene Blends Using Photoinduced Time-Resolved Microwave Conductivity. *J. Phys. Chem. C* **2013**, *117*, 24085−24103.
(33) Israelachvili, J. N.; Mitchell, D. J.; Ninham, B. W. Theory of Self-Assembly of Hydrocarbon Amphiphiles into Micelles and Bilayers. *J. Chem. Soc., Faraday Trans. 2* **1976**, *72*, 1525−1568.
(34) Beaucage, G. Small-Angle Scattering from Polymeric Mass Fractals of Arbitrary Mass-Fractal Dimension. *J. Appl. Crystallogr.* **1996**, *29*, 134−146.
(35) Svergun, D. I.; Koch, M. H. J. Small-Angle Scattering Studies of Biological Macromolecules in Solution. *Rep. Prog. Phys.* **2003**, *66*, 1735−1782.
(36) Choudhary, S.; Bhatia, S. R. Rheology and Nanostructure of Hydrophobically Modified Alginate (HMA) Gels and Solutions. *Carbohydr. Polym.* **2012**, *87*, 524−530.
(37) Svergun, D. I. Restoring Low Resolution Structure of Biological Macromolecules from Solution Scattering Using Simulated Annealing. *Biophys. J.* **1999**, *76*, 2879−2886.
(38) Fairclough, J. P. A.; Norman, A. I. Structure and Rheology of Aqueous Gels. *Annu. Rep. Prog. Chem., Sect. C: Phys. Chem.* **2003**, *99*, 243−276.
(39) Shaw, M. T. *Introduction to Polymer Rheology*; John Wiley & Sons, Inc.: Hoboken, NJ, 2012.
(40) Shah, J. V.; Janmey, P. A. Strain Hardening of Fibrin Gels and Plasma Clots. *Rheol. Acta* **1997**, *36*, 262−268.
(41) Tirtaatmadja, V.; Tam, K. C.; Jenkins, R. D. Superposition of Oscillations on Steady Shear Flow as a Technique for Investigating the Structure of Associative Polymers. *Macromolecules* **1997**, *30*, 1426−1433.
(42) Hyun, K.; Wilhelm, M.; Klein, C. O.; Cho, K. S.; Nam, J. G.; Ahn, K. H.; Lee, S. J.; Ewoldt, R. H.; McKinley, G. H. A Review of Nonlinear Oscillatory Shear Tests: Analysis and Application of Large Amplitude Oscillatory Shear (LAOS). *Prog. Polym. Sci.* **2011**, *36*, 1697−1753.
(43) Hyun, K.; Kim, S. H.; Ahn, K. H.; Lee, S. J. Large Amplitude Oscillatory Shear as a Way to Classify the Complex Fluids. *J. Non-Newtonian Fluid Mech.* **2002**, *107*, 51−65.
(44) Mason, T. G.; Bibette, J.; Weitz, D. A. Yielding and Flow of Monodisperse Emulsions. *J. Colloid Interface Sci.* **1996**, *179*, 439−448.
(45) Evans, R. C. Harnessing Self-Assembly Strategies for the Rational Design of Conjugated Polymer Based Materials. *J. Mater. Chem. C* **2013**, *1*, 4190.
(46) Ferguson, A. J.; Kopidakis, N.; Shaheen, S. E.; Rumbles, G. Dark Carriers, Trapping, and Activation Control of Carrier Recombination in Neat P3HT and P3HT:PCBM Blends. *J. Phys. Chem. C* **2011**, *115*, 23134−23148.
(47) Aguirre, J. C.; Arntsen, C.; Hernandez, S.; Huber, R.; Nardes, A. M.; Halim, M.; Kilbride, D.; Rubin, Y.; Tolbert, S. H.; Kopidakis, N.; et al. Understanding Local and Macroscopic Electron Mobilities in the Fullerene Network of Conjugated Polymer-Based Solar Cells: Time-Resolved Microwave Conductivity and Theory. *Adv. Funct. Mater.* **2014**, *24*, 784−792.
(48) Liang, Z.; Reese, M. O.; Gregg, B. A. Chemically Treating poly(3-Hexylthiophene) Defects to Improve Bulk Heterojunction Photovoltaics. *ACS Appl. Mater. Interfaces* **2011**, *3*, 2042−2050.
(49) Gregg, B. A. Transport in Charged Defect-Rich Π -Conjugated Polymers. *J. Phys. Chem. C* **2009**, *113*, 5899−5901.
(50) Prins, P.; Grozema, F.; Schins, J.; Patil, S.; Scherf, U.; Siebbeles, L. High Intrachain Hole Mobility on Molecular Wires of Ladder-Type Poly(p-Phenylenes). *Phys. Rev. Lett.* **2006**, *96*, 146601.

DOI: 10.1021/acs.jpcb.6b02202
J. Phys. Chem. B 2016, 120, 6215−6224